Thermal Analysis and Design of a 30kW EV Wireless Charger with Liquid-Cooled Shell for Magnetic Coupler and Power Converter Integration

Baokun Zhang, Junjun Deng*, Lantian Li, Zhenpo Wang, Shuo Wang
Department of Mechanical Engineering
Beijing Institute of Technology
Beijing, China
*Email: dengjunjun@bit.edu.cn

Giuseppe Guidi
SINTEF Energy Research
Trondheim, Norway

***Abstract*—The thermal performance affects the reliability and safety of the inductive power transfer system. This paper studies the thermal design process and method of wireless charger for electric vehicle. The thermal resistance of materials is calculated, and the thermal networks of heating components are established. Then power losses are applied to the nodes in the form of heat sources. The calculated hotspot temperatures are close to those obtained by finite element method by comparison. A prototype of 30kW onboard wireless charger with liquid-cooled shell is set up, and the steady-state temperature error of less than 10% proves the effectiveness of the thermal design scheme. This paper expands the application of thermal network method in the field of wireless charging.**

Keywords—thermal design, thermal network method, inductive power transfer, wireless charger

I. INTRODUCTION

Thermal design is quite important for the normal operation of wireless charging system, especially for high-power and compact wireless chargers. However, only in recent years that this field has gained attention. To ensure the thermal balance of the wireless charger in a confined enclosure, the thermal feasibility needs to be rapidly evaluated in the preliminary stage of thermal design. The most widely used approach employed in thermal design is finite element method (FEM). Power losses are calculated and imposed to the finite element model as heat source inputs to obtain the temperature distribution of components [1]. To obtain more accurate loss and temperature, thermal and magnetic field simulation are coupled using FEM [2]–[4]. In addition, computational fluid dynamics (CFD) and FEM are proposed to study the air-cooling conditions [5] and multi-physical field characteristics [6] of the system. The accuracy of FEM is high, but the calculation is time-consuming and the use is complicated. This is especially true in the early thermal design stage where multiple schemes need to be quickly evaluated.

Instead, thermal network method (TNM) is suitable for early evaluation, rapid verification and analysis in engineering applications due to its advantages of simplicity, flexible nodes selection, and less calculation time. TNM has been used to calculate the temperature rise of motors [7], [8]. For the conventional power transformer composed of windings and E type or U type magnetic cores, the thermal network has been proposed in [9]–[11]. As for the application in wireless charging, the thermal resistance model of the receiver is presented in [12], but it is only a schematic diagram, and researchers still rely on FEM to obtain temperature of components. To accelerate the computations used in the optimization process, the maximum surface-related power loss density $p_{v,max}$ is adopted as thermal limit[13], [14]. Furthermore, simplified thermal networks of magnetic core and coil as well as capacitor and heatsink [15] have been established. In the end, FEA is used for simulation to ensure the thermal feasibility .

This work was supported by the National Key Research and Development Program of China (No. 2019YFE0104700)

Considering the issues of the current research, it can be found that TNM is more suitable for the preliminary thermal design and evaluation than FEM. However, it is rarely used in wireless charging system, and mainly exists in the form of qualitative concept map, so it cannot be applied in engineering. Besides, most studies focus on air cooling method, and the scheme using liquid cooling in high-power system has not been studied. To supplement the above deficiencies, this paper takes the onboard wireless charger for electric vehicle as the research object, studies the thermal design and modeling methods, and expands the application of TNM in the field of wireless charging. In Section II, thermal design process of wireless charging system is proposed, and the topology, specifications, and parameters of IPT system are introduced. In Section III, power losses are modeled. Thermal design and analysis of heating components are carried out in Section IV. Simulation and experiment results are shown and discussed in Section V. Finally, key conclusions are drawn in Section VI.

II. THERMAL DESIGN PROCESS AND SYSTEM PARAMETERS

Combined with the design experience of wireless charging system, a detailed flow chart of thermal design progress for IPT system is proposed in Fig 1.

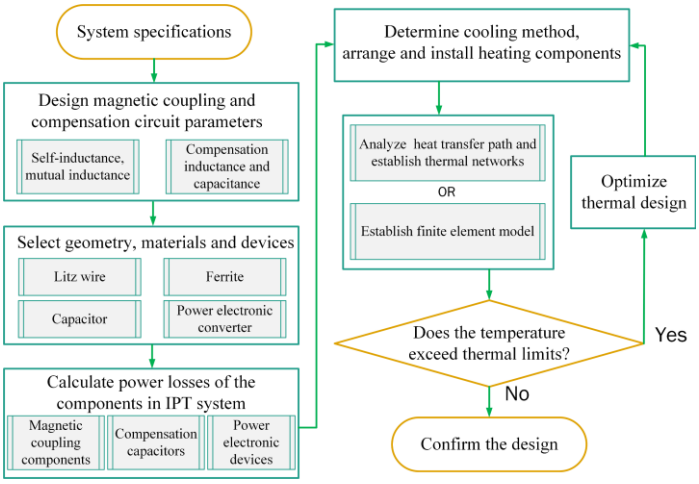

Figure 1. Thermal design process of IPT system for EV

This is the accepted version of an article published in 2021 IEEE Applied Power Electronics Conference and Exposition - APEC
http://dx.doi.org/10.1109/APEC42165.2021.9487097

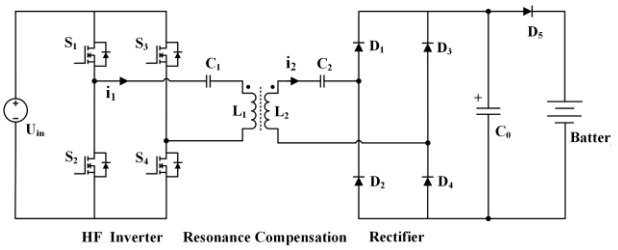

Figure 2. Schematic diagram of the IPT system

TABLE I. PARAMETERS OF THE IPT SYSYTEM

Parameter	Value
Rectangular winding size(mm)	440 ×380
Number of turns	10
Self-inductance (μH)	75.1
Mutual inductance (μH)	13.4
Ferrite core size (mm)	540×390×15
Compensation capacitors(μF)	7×0.33
Air gap (mm)	170
Frequency (kHz)	85

Taking a set of 30kW IPT system as an example, the thermal design and experimental verification are carried out according to the flowchart. Firstly, S-S compensation topology is adopted and the schematic diagram of IPT system is shown in Fig 2. Transmission frequency and air gap are chosen according to the standard SAE J2954. To transfer rated power, proper self-inductance and mutual inductance should be designed properly. As for compensation capacitances, they could be obtained as long as the compensation topology is determined. According to voltage grade and current density, the materials of Litz wire, ferrite, compensation capacitors as well as power electronic devices are selected.

Because of limited space, the design and optimization of resonant circuit parameters are not shown in this paper. After finite element simulation and circuit simulation in the preliminary design stage, the specifications and parameters of the IPT system are listed in Tab I. It's pointed out that identical winding, ferrite cores as well as compensation capacitors are chosen for simplicity.

III. MODELING & CALCULATION OF POWER LOSSES

The system power losses consist of: (a) magnetic coupling components (Litz wire, ferrite core, aluminum), (b) compensation capacitors, and (c) power electronics devices (mosfet, diode) [16]. They are briefly discussed in the following.

At the transmission frequency of 85 kHz, the skin depth δ is around 0.23mm. To significantly reduce the power losses generated by skin effect, the Litz wire strand diameter is selected as 0.1mm. And strand number is 2500 to ensure sufficient current carrying capacity. Nevertheless, the proximity effect losses can't be ignored, and the ac-to-dc resistance ratio k_{ac-dc} is used to describe this effect. The winding copper losses can be calculated by

$$P_{loss\_winding} = I_{rms}^2 R_{dc} \cdot k_{ac-dc} \quad (1)$$

Where R_{dc} and k_{ac-dc} can be estimated according to the table provided by manufactures once the number of strands and frequency are determined, and I_{rms} is the effective value of the current flowing through the winding.

The power losses in the employed ferrite cores can be calculated by the integration of core loss density p_{core} over the volume of cores in FE tool. And Steinmetz equation is as follows.

$$P_{loss\_core} = C_m f^{\alpha} \hat{B}^{\beta} \quad (2)$$

where $\hat{B}$ is the peak magnetic flux density. C_m, α, and β are three coefficients of the ferrite material, which are typically provided by the material manufacture.

Similarly, the eddy current losses on the aluminum liquid-cooled shell can be obtained from the FE tool.

For polypropylene film capacitors of type CSP 120/200, due to their voltage rating, a series connection of seven devices is required through copper busbars. Dissipation factor $\tan\delta$ is the key parameter in modeling the capacitor losses, and its value is around 1.4×10^{-3} at selected frequency.

$$P_{loss\_cap} = \tan\delta \cdot I_{rms}^2 \big/ 2\pi f \cdot C \quad (3)$$

The power electronic losses of onboard wireless charger are mainly caused by the rectifier. SiC schottky diode of type C4D40120D are used for the high-frequency operation and 1.2kV voltage class. And each switch is composed of two discrete devices in parallel. The switching and conduction losses are computed using the data provided in the manufacture's datasheet and equations presented in [17].

IV. THERMAL ANALYSIS AND THERMAL NETWORK

In this section, employed theory and formulas of heat transfer are introduced. After that, the cooling method, arrangement and installation of heating components are designed. In terms of the proposed thermal design scheme, heat transfer path and temperature rise of components are analyzed using TNM.

A. Basic theory and formulas of heat transfer

The heat transfer mechanisms are conduction, convection, and radiation. In this paper, only conduction and convection are considered. The steady state temperature of the system is more concerned in the thermal design process and the thermal behavior is characterized by a single resistance R_{th}. The formulas to determine resistance are given as follows.

In the mechanism of conduction, for a cube with conduction length L, cross section A, and thermal conductivity k, its thermal resistance inside the material can be calculated by

$$R_{th\_cd} = L \big/ kA \quad (4)$$

In the mechanism of convection, the thermal resistance between the surface and the ambient can be calculated by

$$R_{th\_cv} = 1 \big/ h_{conv} A_{surf} \quad (5)$$

This is the accepted version of an article published in 2021 IEEE Applied Power Electronics Conference and Exposition - APEC
http://dx.doi.org/10.1109/APEC42165.2021.9487097

Where h_{conv} is the convection coefficient of the surface and A_{surf} is the area of exposed surface.

When we calculate the heat transfer convection coefficient between flow channels and liquid coolant, the relevant formulas of fluid dynamics and heat transfer are shown below.

For liquids flowing in flow channels, its Reynolds number and Prandtl number are calculated by

$$\mathrm{Re} = \rho V L \big/ \mu \tag{8}$$

Where V is mean flow rate, μ is hydrodynamic viscosity, ρ is fluid density, L is equivalent diameter of the flow channel.

$$\mathrm{Pr} = \mu c \big/ \lambda \tag{9}$$

Where c is the specific heat at constant pressure and λ is the thermal conductivity of liquid coolant.

If Re is between 2100 and 10000, heat transfer factor j follows the equation[18]

$$j = 0.116\,(\mathrm{Re}^{\frac{2}{3}} - 125) \Big/ \mathrm{Re} \tag{10}$$

If Re is more than 10000, heat transfer factor j follows the equation

$$j = 0.023 \Big/ \mathrm{Re}^{0.2} \tag{11}$$

Then convection coefficient α can be calculated by

$$\alpha = j \cdot g_m \cdot c \cdot \mathrm{Pr}^{-\frac{2}{3}} \tag{12}$$

Where g_m is mass velocitsy of liquid coolant.

B. Thermal design of components

Conventional onboard wireless chargers typically have only magnetic coupling components inside, while compensation capacitors and power converters are placed outside. Nevertheless, in this IPT system all these components are integrated into the shell of onboard wireless charger. The integrated design makes full use of the limited space under the chassis to achieve compactness. In addition, the energy transmission components and the power convert devices make a whole, and DC is drawn directly from the interface of onboard wireless charger. From the point of view of thermal design, it's convenient for uniform and integrated cooling of heating components.

Fig 3 shows the inner arrangement of components in onboard wireless charger. The rectangular winding and ferrite cores are closely adjacent to improve the magnetic properties. The coil frame attaches the Litz wire winding tightly to the ferrite cores in the middle, and the four edges of the cores are fixed to the liquid-cooled plate by the ferrite fixture. The compensation capacitors are fixed on the liquid-cooled plate by a fixture. The inner surface of the fixture is equipped with thermally conductive interface pads (also known as thermal pads), so as to realize high-voltage insulation and heat conduction. The rectifier diodes are fixed on the aluminum plate and then mounted on the liquid-cooled plate. The flow channel is evenly distributed under the above components. Finally, the shell is sealed with plastic covers, and the air inside is not flowing.

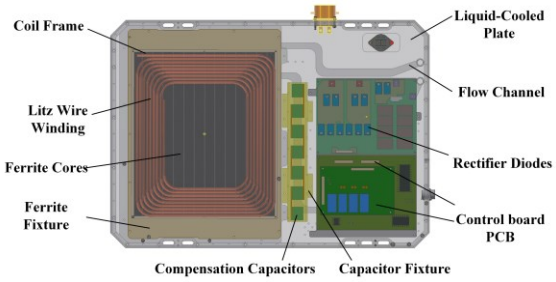

Figure 3. Layout of inner components in wireless charger

TABLE II. THERMAL CHARACTERISTICS OF KEY MATERIALS

Component	Thermal conductivity (W/mK)	Thermal limit (℃)
Ferrite core	4	120
Litz wire	1	155
Metallized film dielectric	43.6	90
Diode	\	175

The heat transfer from hotspots to the ambient takes several different paths, and each path is composed of series and or parallel thermal resistances. Then the power losses are applied to the nodes of two-dimensional thermal networks in the form of point heat sources, and temperature rise can be calculated. It's easy to understand the principle of thermal design is to provide heat transfer paths whose thermal resistance is as low as possible. Besides, key components and their thermal characteristics are summarized in Tab II.

In order to simplify the thermal model, three assumptions are made. First, thermal contact resistance is ignored, and the surfaces of components fit together as closely as possible by adding thermal interface materials or applying external force. Second, characteristic parameters like thermal conductivity and resistivity are temperature dependent. But for simplicity, the thermal characteristic parameters at room temperature are adopted. Third, thermal cross coupling effects are not considered because each component in the model is basically independent.

C. Thermal analysis and thermal network

1) Litz wire winding and ferrite cores

The served Litz wire winding is sticked to the coil frame with a thin layer of hot melt adhesive, with potting compounds on the other side. When modeling their radial thermal resistances, the contact area between the winding and hot melt adhesive or potting compounds is considered to be 60% of the wire cross-sectional area. Polyimide tape provides electrical insulation at high temperature, so it's used in many positions inside the wireless charger. Because the onboard shell is mounted upside down, there will be a tiny air gap between ferrite cores and liquid-cooled plate under the action of gravity.

Assume that hotspot temperatures are homogeneous and occur in the central plane of the winding and cores, respectively. Then suppose that the material is symmetric about the central plane, and equal models are assumed for the top and bottom

This is the accepted version of an article published in 2021 IEEE Applied Power Electronics Conference and Exposition - APEC
http://dx.doi.org/10.1109/APEC42165.2021.9487097

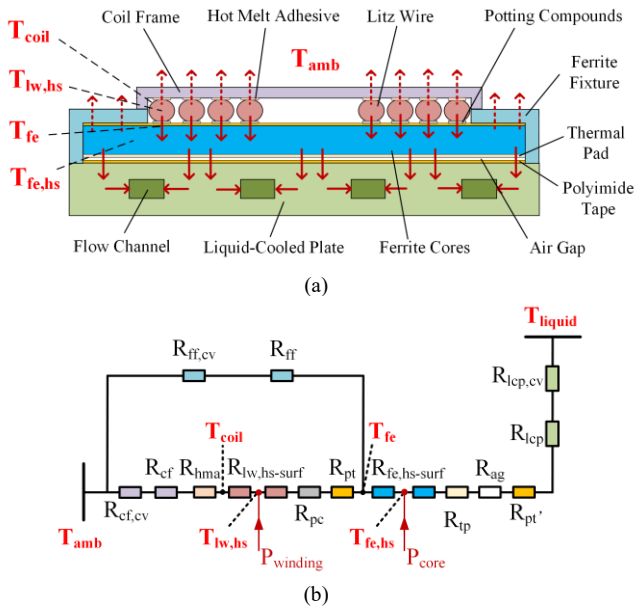

Figure 4. Thermal analysis and modeling of Litz wire winding and ferrite cores (a) heat transfer path (b)thermal network

winding surfaces as well as ferrite cores surfaces. Due to the limited side area of winding and ferrite cores, the path of side heat transfer is not considered.

As shown in Fig 4(a), the direction of arrows indicates the transfer path of winding losses and core losses, and the thermal network is established accordingly in Fig 4(b). The thermal resistance $R_{lw,hs-surf}$ models the heat conduction from the hotspot inside the winding to the winding surface and R_{pc} models the heat conduction from one side to the other of potting compounds. R_{lcp} models the heat conduction from the vertical plane of heat sources to the central vertical plane of the nearby flow channel. While $R_{lcp,cv}$ models the heat convection between the wall of flow channel and liquid coolant, and others are similar.

Note that the temperature of liquid coolant is not always the same, as the coolant passes through more components, its temperature increases. And the temperature rise from inlet to the specific position can be calculated by the following formula.

$$T_{liquid} - T_{inlet} = \sum P_i \Big/ c\,\dot{m} \tag{13}$$

Where $\sum P_i$ is the sum of power losses of components which have been passed through, and $\dot{m}$ is the mass flow of coolant.

By calculation, it's obvious that most winding losses and core losses are transferred down to the liquid-cooled plate by conduction, and taken away by liquid coolant, while the heat dissipation to the air inside the shell is little, which proves the significance of liquid cooling. The main heat transfer path is shown in the form of solid arrows while others are dotted arrows, and the same is true to other thermal networks.

2) Compensation capacitors

The capacitors and installation environment is symmetric about the center plane, therefore, only the left side of a capacitor is analyzed. Considering the material of electrodes and busbars are all copper and they are regarded as whole. We estimate that 50% of capacitor bank losses are evenly distributed in the dielectric and others are distributed evenly in copper electrodes and busbars. They are regarded as point heat sources and hotspot positions inside the material, and hotspot temperatures are $T_{mfd,hs}$ and $T_{cu,hs}$, respectively.

Heat transfer path of dielectric losses and copper losses is illustrated in Fig 5(a). Most heat is transferred to the liquid-cooled plate and only a small fraction of the heat is transferred to the air inside the shell by conduction and convection, which is similar to the case of winding and ferrite cores. Fig 5(b) shows the thermal network, where R_{mfd-x} models heat conduction of metallized film dielectric in the horizontal plane, while R_{mfd-z} models heat conduction in the vertical plane. And others are similar.

3) Rectifier diodes

The rectifier diodes as well as rectifier PCB is mounted on a 4mm-thick aluminum plate, between which thermal grease, alumina ceramics heat conducting sheets and thermal grease are applied to enhance the heat conducting effect. For similar reasons, thermal pads are employed between aluminum plate and liquid-cooled plate. The junction temperature T_j is commonly regarded as the hotspot temperature of diodes. The heat transfer path and thermal network are illustrated in Fig 6(a) and 6(b). R_{jc} models the thermal resistance from junction to the case. As an important property parameter, it can be looked up in the datasheet. By calculation, it's evident that the thermal resistance of thermal pads and thermal grease (R_{tp} *and* R_{tg}) has

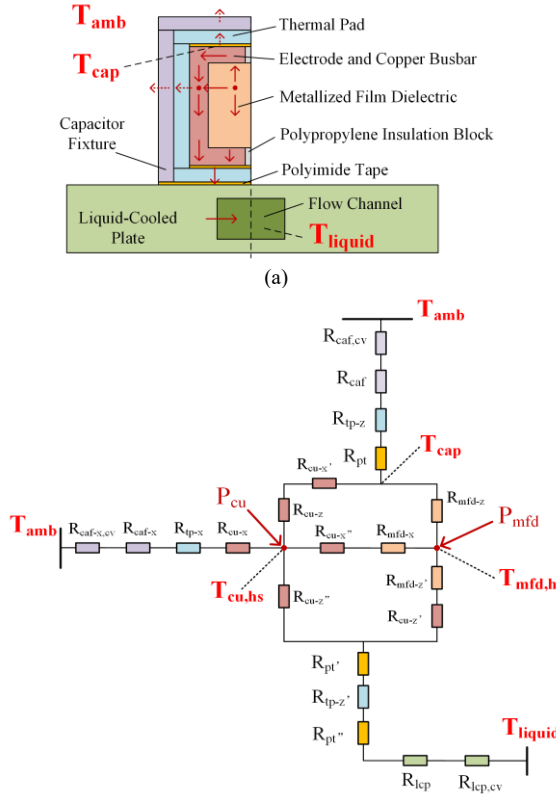

Figure 5(b). Thermal analysis and modeling of the compensation capacitor (a) heat transfer path (b) thermal network

This is the accepted version of an article published in 2021 IEEE Applied Power Electronics Conference and Exposition - APEC
http://dx.doi.org/10.1109/APEC42165.2021.9487097

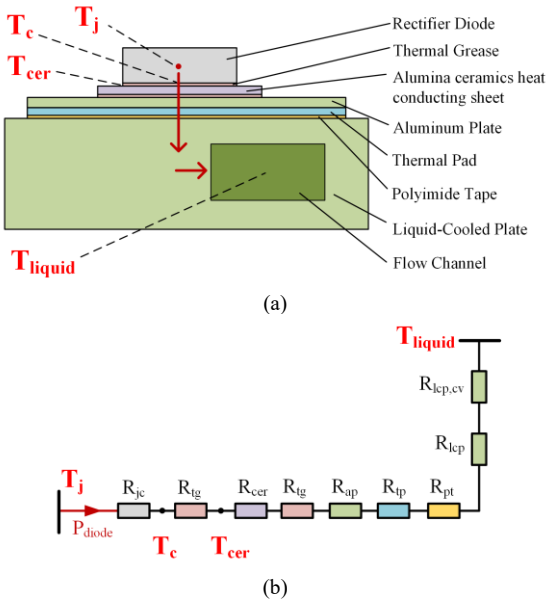

Figure 6(b). Thermal analysis and modeling of the rectifier diode (a) heat transfer path (b) thermal network

a great effect on the temperature rise of diodes, and attention should be paid to the choice of their material and thickness.

D. *Working conditions and others*

The working conditions of the wireless charger are summarized in Tab III. Eddy losses are distributed in the liquid-cooled plate, and most of them are conducted to flow channels easily due to the high thermal conductivity of aluminum. Therefore, it has little effect on the temperature of Litz wire and so on, and they are ignored in the thermal network but considered in finite element model.

To sum up, the liquid-cooled method relies on heat conduction and fluid convection to carry heat away, while internal air convection carries away limited heat.

V. SIMULATION AND EXPERIMENT VERIFICATION

In this section, FEM is adopted to make a comparison with the results by TNM. Next, the experiment is carried out and the temperature of above components is obtained.

A. *Simulation in FE tool*

In order to verify the feasibility of TNM, corresponding model is established in FE tool. To reduce the required number

TABLE III. WORKING CONDITIONS OF THE WIRELESS CHARGER

Parameters	Value
Ambient temperature (℃)	25
Inlet liquid coolant temperature (℃)	25
Inner ambient temperature (℃)	50
Inner convection coefficient (W/mK)	2
Natural convection coefficient (W/mK)	6 [19]
Liquid coolant flow (L/min)	8

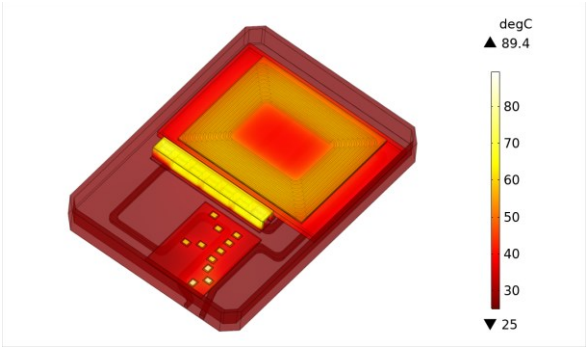

Figure 7. Temperature distribution of onboard wireless charger

of finite element simulations, the feedback of the calculated component temperatures to the power loss calculation is not included. Water is selected as liquid coolant by right of its cheapness and accessibility in simulation as well as in prototype experiment. In addition, Y+ algebraic model of turbulence is employed by virtue of its low calculated strength and good approximation of the internal flow. For better approximation to the actual situation, the losses in the finite element model are uniformly distributed in the volume of winding, cores, and capacitors in the form of heat sources, which is different from the point heat sources in the thermal network. Initial temperature of these components is set to 25℃. The temperature distribution of each component in wireless charger is obtained and illustrated in Fig 7.

The highest temperature of each component is selected as its hotspot temperature. They are summarized and compared in Tab IV. By contrast, the difference between TNM and FEM is less than 10%. This indicates that TNM can be used in the thermal design of wireless charging system, and the accuracy is acceptable.

B. *Experiment*

Onboard wireless charger is built according to the thermal design scheme proposed above. The temperatures are measured with thermocouples and fiber temperature sensors that are glued to the Litz wire, cores, capacitor and ceramics sheet. the position of measurement points are shown in Fig 4 to Fig 6. Note that due to the limitation of the measuring devices, we can only obtain the temperature of material surface or the temperature of adjacent component, rather than the hotspot temperature inside the material. Then we build the experiment set up, as shown in Fig 8. The working conditions are in accord with that of FE model. The output power of the system is kept at 28.6kW, and the dc-dc efficiency is as high as 95.9%. The system basically reaches steady state after working 35 minutes.

TABLE IV. COMPARISION OF HOTSPOT TEMPERATURE OBTAINED BY TNM AND FEM

	$T_{lw,hs}$	$T_{fe,hs}$	$T_{mfd,hs}$	T_j
TNM(℃)	55.3	47.6	67.5	86.1
FEM(℃)	58.9	52.7	69.1	89.4
Difference(%)	6.1	9.7	2.3	3.7

This is the accepted version of an article published in 2021 IEEE Applied Power Electronics Conference and Exposition - APEC
http://dx.doi.org/10.1109/APEC42165.2021.9487097

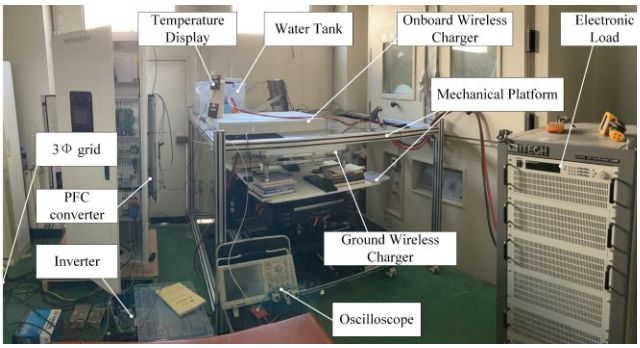

Figure 8. Experimental set up of the proposed IPT system

TABLE V. TEMPERATURE AT THE MEASURED POINT OBTAINED BY TNM, FEM, AND EXPERIMENT

	T_{coil}	T_{fe}	T_{cap}	T_{cer}
TNM	55.2	47.0	66.9	64.2
FEM	57.6	52.0	64.3	60.4
Experiment	58.0	51.4	69.5	66.6

Tab V summarizes the temperature at the measured point obtained by TNM, FEM and experiment. The TNM and FEM show the same performance and are close to the experiment values (the error is less than 10%), indicating the feasibility of the proposed thermal design process and scheme in the field of wireless charging. Considering the simplification and approximation when modeling, the accuracy is sufficient to judge the thermal design schemes and ensure the thermal reliability during operation.

VI. CONCLUSIONS AND FUTURE WORK

A thermal design process of IPT system is proposed, and a 30kW onboard wireless charger prototype is built accordingly. The heat transfer path of the heating components are analyzed and thermal networks are established. By comparing the results by TNM and FEM, the error is less than 10%, proving the feasibility of the TNM in the field of wireless charging thermal design. The experiment results are close to the calculated and simulated results, indicating the effectiveness of the proposed thermal design scheme. Nevertheless, the work presented in this paper only studies the thermal characteristics at the aligned position. Future research could, therefore, explore the thermal performance of the system at misaligned position.

REFERENCES

[1] V. Kindl, R. Pechanek, M. Zavrel, T. Kavalir, and P. Turjanica, "Inductive coupling system for electric scooter wireless charging: electromagnetic design and thermal analysis," Electr. Eng., vol. 102, no. 1, pp. 3–12, Mar. 2020.

[2] S. Niu, H. Yu, S. Niu, and L. Jian, "Power loss analysis and thermal assessment on wireless electric vehicle charging technology: The over-temperature risk of ground assembly needs attention," Appl. Energy, vol. 275, pp. 115344, 2020.

[3] M. Alsayegh, M. Saifo, M. Clemens, and B. Schmuelling, "Magnetic and thermal coupled field analysis of wireless charging systems for electric vehicles," IEEE Trans. Magn., vol. 55, no. 6, pp. 1–4, Jun. 2019.

[4] S. Kim, M. Amirpour, G. Covic, and S. Bickerton, "Thermal characterisation of a double-d pad," in 2019 IEEE PELS Workshop on Emerging Technologies: Wireless Power Transfer (WoW), London, United Kingdom, Jun. 2019, pp. 1–5.

[5] N. Rasekh, S. Dabiri, N. Rasekh, M. Mirsalim, and M. Bahiraei, "Thermal analysis and electromagnetic characteristics of three single-sided flux pads for wireless power transfer," J. Clean. Prod., vol. 243, pp. 118561, Jan. 2020.

[6] M. Moghaddami and A. Sarwat, "Time-dependent multi-physics analysis of inductive power transfer systems," in 2018 IEEE Transportation Electrification Conference and Expo (ITEC), Long Beach, CA, USA, Jun. 2018, pp. 130–134.

[7] A. Boglietti, A. Cavagnino, M. Lazzari, and A. Pastorelli, "A simplified thermal model for variable speed self cooled industrial induction motor," in Conference Record of the 2002 IEEE Industry Applications Conference. 37th IAS Annual Meeting (Cat. No.02CH37344), Pittsburgh, PA, USA, 2002, vol. 2, pp. 723–730.

[8] J. Wang, X. Wang, Y. Ma, N. Liu, and Z. Yang, "Analysis of heat transfer in power split device for hybrid electric vehicle using thermal network method," Adv. Mech. Eng., vol. 6, pp. 210170, Jan. 2014.

[9] E. Snelling, Soft Ferrites Properties and Applications. London: Iliffe Books Ltd, 1969, pp. 303-305.

[10] V. C. Valchev and A. Van den Bossche, Inductors and Transformers for Power Electronics, 1st ed. CRC Press, 2005, pp. 258-263.

[11] R. Petkov, "Optimum design of a high-power, high-frequency transformer," IEEE Trans. Power Electron., vol. 11, no. 1, pp. 33–42, Jan. 1996.

[12] C. Liang et al., "Modeling and analysis of thermal characteristics of magnetic coupler for wireless electric vehicle charging system," IEEE Access, vol. 8, pp. 173177–173185, 2020.

[13] R. Bosshard, J. W. Kolar, J. Muhlethaler, I. Stevanovic, B. Wunsch, and F. Canales, "Modeling and η-α-pareto optimization of inductive power transfer coils for electric vehicles," IEEE J. Emerg. Sel. Top. Power Electron., vol. 3, no. 1, pp. 50–64, Mar. 2015.

[14] R. Bosshard, "Multi-objective optimization of 50 kw/85 khz ipt system for public transport," IEEE J. Emerg. Sel. Top. POWER Electron., vol. 4, no. 4, pp. 13, 2016.

[15] R. Bosshard, "Multi-objective optimization of inductive power transfer systems for EV charging," ETH Zurich, 2015, pp.132-134.

[16] S. Bandyopadhyay, "Comparison of magnetic couplers for ipt-based ev charging using multi-objective optimization," IEEE Trans. Veh. Technol., vol. 68, no. 6, pp. 14, 2019.

[17] K. Peng and E. Santi, "Performance projection and scalable loss model of SiC MOSFETs and SiC Schottky diodes," in 2015 IEEE Electric Ship Technologies Symposium (ESTS), Old Town Alexandria, VA, USA, Jun. 2015, pp. 281–286.

[18] W. McAdams, Heat Transmission, 3rd ed. New York-London: Krieger Pub Co, 1954, pp.237-241.

[19] J. Biela and J. W. Kolar, "Cooling concepts for high power density magnetic devices," IEEJ Trans. Ind. Appl., vol. 128, no. 4, pp. 500–507, 2008.

This is the accepted version of an article published in 2021 IEEE Applied Power Electronics Conference and Exposition - APEC
http://dx.doi.org/10.1109/APEC42165.2021.9487097